A REPRINT FROM THE OCTOBER 1993 ISSUE OF

AIChE JOURNAL

A COMBINED HEAT-TRANSFER ANALYSIS OF A SINGLE-FIBER CVD REACTOR

M. Kassemi, S. A. Gokoglu,
C. H. Panzarella, and L. C. Veitch

NASA Lewis Research Center
Cleveland, OH 44135

A Combined Heat-Transfer Analysis of a Single-Fiber CVD Reactor

M. Kassemi, S. A. Gokoglu, C. H. Panzarella, and L. C. Veitch
NASA Lewis Research Center, Cleveland, OH 44135

A combined-conjugated heat-transfer and fluid-flow analysis is presented for coating fibers by CVD in a vertical cylindrical quartz reactor. The numerical model focuses on radiation and natural convection. Three case studies are performed, and the wall temperature predictions are compared to experimental measurements. In the first case, the flowing gas is hydrogen, and conduction is more important than both radiation and convection, in which case measured and predicted wall temperatures agree excellently. In the second, hydrogen is replaced by argon, thus making radiation heat transfer more important than the previous situation. Three radiation models with increasing degrees of sophistication are compared: an approximate nongray model (no wavelength dependence of emissivity), an approximate semigray model, and a rigorous semigray model with view factor calculations. Comparison with experiments suggest that a semigray radiative analysis is needed for correct determination of wall temperatures. The third involves argon at a lower flow rate, where natural convection effects are more pronounced. Checking the validity of the Boussinesq approximation by incorporating the explicit dependence of density on temperature in the model shows a slight difference between the velocity fields predicted using the Boussinesq approximation and those obtained using the explicit dependence of density on temperature. However, there is negligible difference between the temperature fields predicted in the two cases.

Introduction

The reliability of advanced ceramics used as high-temperature structural materials is a major concern of the aeropropulsion industries. In these high-temperature applications, structural fibers such as SiC are currently being considered for reinforcement of both ceramic and intermetallic matrices. Among the methods available for fabricating structural fibers from the gas phase, the CVD technique, which has been traditionally used for preparation of optical and electronic materials, has proved to be extremely versatile. Because the CVD technique is economical to develop and easy to scale up, it is also very suitable for commercial applications.

In general, structural materials have not received the same degree of attention in terms of the precision of the CVD process as electronic and optical materials. However, as these materials are expected to withstand more stringent conditions, it is clear that a sound understanding of the interactive physicochemical and transport phenomena which control the CVD process is needed for better control of the fabrication procedures. This understanding can be achieved best through a combined numerical and experimental approach, in which the effects of the various interacting phenomena are isolated.

To this end, a cold-wall CVD reactor was constructed at NASA Lewis to study coating of stationary monofilament fibers. This process was chosen because of its relevance to the fabrication of Textron's SCS-6 silicon carbide fibers. The experimental effort is complemented by numerical modeling. In this reactor, where the hot fiber is kept at a relatively uniform temperature and the reactor walls are passively cooled, there are two major sources of difficulty. First is the recirculation of the gas due to secondary natural convection flow which increases the residence time of the gases in the reactor and can cause gas-phase nucleation. Second is the increase in reactor wall temperature which can cause deposition on the wall. Both of these factors affect the quality of the coating and the efficiency of the process. Consequently, there is a strong need for accurate prediction of fluid flow and temperature fields in

the CVD reactor. Needless to say, accurate predictions of flow and temperature fields are also essential for correct determination of chemistry and proper accounting of the gas-phase chemical species.

To date, most of the sophisticated CVD models have been applied to the preparation of electronic materials. Reviews of the current status in CVD modeling have been given by Jensen (1989) and Gokoglu (1990). Unfortunately, the existing literature on modeling of transport phenomena governing deposition on structural fibers is by no means extensive. Other than the simplified approaches of Revankar et al. (1988) for cold-wall and Alam (1991) for hot-wall reactors, the literature seems to consist of the works done by Scholtz et al. (1990, 1991) for boron deposition and Gokoglu et al. (1989, 1990) for cold-wall reactors. The applications of CVD modeling to high-temperature structural materials are discussed by Gokoglu (1991).

A review of these works identifies two areas which have to be examined in more detail. *First is radiation heat transfer between the heated fiber and the quartz reactor wall.* Quartz is a spectrally selective material, essentially transparent to radiation below wavelengths of 3 micron and almost opaque to infrared radiation. At high fiber temperatures, a large portion of the radiation emitted by the fiber is within the transparent band. Consequently, a nongray analysis is necessary to account for the radiative exchange within the enclosure. *Second is the effect of natural convection.* Due to the large temperature differences in the reactor, two different models for temperature-dependent density are compared: the familiar Boussinesq approximation and an explicit temperature-dependent density model.

As an integral part in the development of a high-fidelity numerical model for coating of fibers by CVD, this article will focus on both of these issues. The complicating effects of species transport and chemistry will be addressed in future works.

Experimental Procedure and Apparatus

The experimental reactor is a vertically oriented cylindrical quartz tube which is shown sideways in Figure 1. At the inlet of the reactor the gases pass through a porous carbon felt which dampens the complicated entrance effects and produces a relatively uniform inlet flow. The inlet and exit blocks are made of brass and are water-cooled. The reactor wall is not actively cooled, but left open to the surrounding environment. Textron SCS-6 silicon carbide fibers (140 micron in diameter) are used as the deposition substrate. There are mercury pools at the top and bottom of the reactor, and the fiber is inserted into the reactor through these pools. The mercury is held by surface tension and provides sealing and electrical contacts for the resistively heated fiber. The system can accommodate variable fiber lengths, but is currently limited to electrically conducting single fibers for atmospheric pressure operation. This design is suited for possible continuous operation in the future.

The reactor wall temperatures are measured by chromel-alumel thermocouples which are surface-mounted at 1, 2, 3, 4, 5, 10, 15 and 20 cm from the inlet of the tube. The inlet is defined as the location where the fiber emerges from the bottom mercury pool (0 cm). The small thermal inertia of thermocouples (12.7 micron junction thickness) yields fast response.

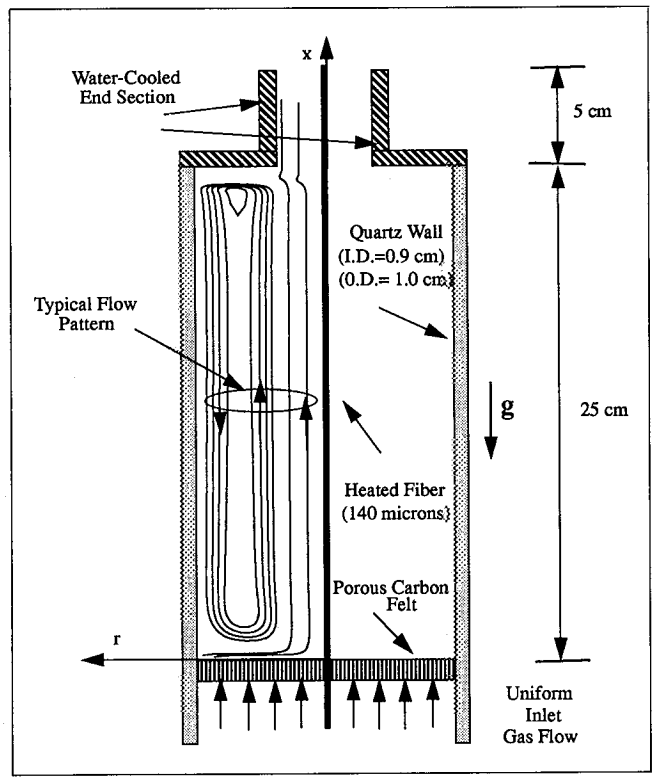

Figure 1. Vertical fiber growth reactor.

The temperature readings are automatically recorded by a data acquisition system. Fiber temperature is measured by a dual-wavelength optical pyrometer, rated for measurements above 900°C.

Mathematical Model

The fiber growth reactor is modeled as an axisymmetric cylinder. Flow in the reactor is described by the continuity and momentum equations which are written as:

$$\nabla \cdot \rho \vec{u} = 0 \tag{1}$$

$$\rho[\vec{u} \cdot \nabla \vec{u}] = -\nabla p + (\rho - \rho_0)\vec{g} + \nabla \cdot [\mu(\nabla \vec{u} + \nabla \vec{u}^T)] \tag{2}$$

Because of the large temperature differences between the heated fiber and the quartz wall, the density of the fluid is described by the ideal gas law. In this formulation, the dependence of density on temperature is incorporated explicitly in all terms of Eq. 2. The other thermophysical properties of the fluid are also temperature-dependent. This case is referred to as the variable density model in the text. For comparison, the traditional Boussinesq approximation is also used in the last example presented here. In this case, referred to as the Boussinesq model, density is constant ($\rho = \rho_o$) in all the terms of Eq. 2 except in the buoyancy term where it is represented by:

$$\rho = \rho_o[1 - \beta_T(T - T_o)] \tag{3}$$

Equation 2 is subject to the nonslip boundary condition at all the enclosing surfaces. There are two main driving forces

for the flow. The first is the uniform velocity at the inlet. This assumption is a suitable description of the experimental setup which uses flow straighteners to smooth the initial disturbances at the reactor entrance. In any case, numerical experimentation has shown that because the flow adjusts itself to the nonslip condition at the wall within several grid steps, the solution is not sensitive to the flow distribution imposed at the inlet. The second driving force is the buoyancy term which couples the momentum and energy equations. The energy equation for fluid is written as a balance between convection and conduction:

$$\rho c_p[\vec{u}\cdot\nabla T]=\nabla\cdot(k\nabla T) \tag{4}$$

The working fluids are either argon or hydrogen. They have temperature-dependent thermophysical properties. In accordance with the experimental conditions, the water-cooled inlet and outlet sections of the reactor are kept at constant temperatures of 300 K. Since the working fluids are assumed to be transparent, radiation exchange within the reactor takes place only between the quartz wall and the heated fiber.

The cylindrical quartz wall is assumed to be conducting in both the radial and axial directions (although results show that because the wall is very thin, the radial temperature gradients are insignificant). Due to the coupling between the fluid and the wall energy equations, a conjugated heat-transfer situation exists. The wall energy is written as:

$$\nabla\cdot(k_w\nabla T_w)=0 \tag{5}$$

Quartz is considered to have temperature-dependent thermal properties. For the cylindrical wall, the inside boundary condition is determined by a balance among radiation, conduction, and convection:

$$\hat{n}_i\cdot k_w\nabla T_w=\hat{n}_i\cdot k\nabla T-q_{w_i} \tag{6}$$

In the above representation, q_{w_i}, is the net radiative flux which will be described shortly.

The cylindrical wall loses heat via radiation and convection to the outside environment. Therefore, the outside wall thermal boundary conditions are represented by a balance among conduction, convection, and radiation as:

$$\hat{n}_o\cdot k_w\nabla T=h_c(T_w-T_\infty)+q_{w_o} \tag{7}$$

The convective loss to the surrounding is modeled using a heat-transfer coefficient h_c which for natural convective flows over cylindrical bodies can be written as:

$$h_c=\frac{k}{x}\left[0.678Ra_x^{1/4}\left(\frac{Pr}{0.952+Pr}\right)^{1/4}\right] \tag{8}$$

This is a modified version of the correlation presented in Lienhard (1989). To check the validity of the above correlation, convection over the reactor was modeled by extending the mesh beyond the reactor wall and applying the full Navier-Stokes equations to the outside air flow. The convective heat-transfer coefficient computed from this simulation was in excellent agreement with the correlation presented above. Therefore, relation 8 was used for all of the cases presented here to save computation time.

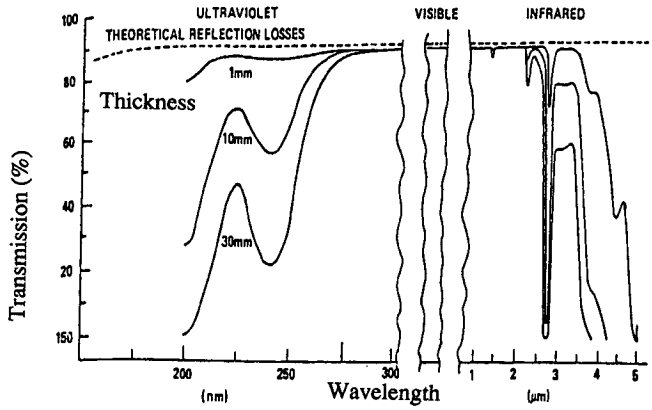

Figure 2. Spectral transmission of quartz (Holland, 1980).

The term, q_{w_i}, in Eq. 6, represents the net radiative heat transfer at the inside of the quartz wall. Quartz is a radiatively selective material with a sharp drop in transmission from 95% to almost 0% in the 3–5 micron wavelength range, as shown in Figure 2. There is also a 5% reflection at all wavelengths. As a result, quartz absorbs all of the infrared radiation and transmits the radiation in the visible range. For a fiber at 1,700 K, about 75% of the total emitted radiation is in the transparent band of quartz. Therefore, a spectral radiation analysis is essential for a correct representation of radiative transfer in the CVD reactor.

In this work, a semigray approach is adopted in which the transmittance of quartz is assumed to undergo a step change at a cutoff wavelength of λ_c. To simplify the analysis, the 5% reflectance of quartz is neglected across the entire wavelength range and a two-band model is formulated with a band limit of λ_c where:

$$\epsilon_w=0 \quad \text{for} \quad \lambda<\lambda_c \tag{9}$$

$$\epsilon_w=1 \quad \text{for} \quad \lambda>\lambda_c \tag{10}$$

and according to Figure 2, λ_c can vary anywhere between 3 to 5 micron.

Three different models with increasing degree of complexity are used to represent radiative heat transfer in the reactor. The most rigorous formulation, referred to as RAD I, divides the surface of the fiber and the quartz enclosure into small areas (matching the flow and heat-transfer mesh), and a semigray diffuse analysis is applied to the enclosure. The resulting relationships are as follows:

$$q_{w_i}=W_w-H_w \tag{11}$$

$$W_w=\epsilon_w F(\lambda_c,\ T_w)\sigma T_w^4+(1-\epsilon_w)H_w \tag{12}$$

$$H_w=\int\int_{A_w} W_w(r,r')K_{w,w}(r,r')dA + \int\int_{A_f} W(r,r')K_{f,w}(r,r')dA \tag{13}$$

where W and H are the outgoing and incoming radiosities, respectively, and K represents the view factor kernel. The second radiation model, RAD II, assumes, that for radiation purposes, the reactor and the fiber can be represented by two infinite concentric cylinders at uniform temperatures. Therefore, a much simpler expression is derived for q_{w_i} which still retains the full effect of the semigray analysis:

$$q_{w_i} = [1 - K_{w,w} - (1-\epsilon_f)K_{f,w}K_{w,f}]F(\lambda_c, T_w)\sigma T_w^4 - \epsilon_f K_{w,f} F(\lambda_c, T_f)\sigma T_f^4 \quad (14)$$

The last and the least sophisticated model, RAD III, represents a nongray radiation analysis again for infinite concentric cylinders. It is also represented by Eq. 14 with the cutoff wavelength, λ_c, set to zero. According to RAD III, the quartz wall is assumed to be opaque to thermal radiation over the entire wavelength spectrum.

Finally, in all three radiation models, the net radiative heat transfer at the outside surface of the quartz wall is represented by:

$$q_{w_o} = \epsilon_w \sigma [F(T_w, \lambda_c) T_w^4 - F(T_\infty, \lambda_c) T_\infty^4] \quad (15)$$

Numerical Formulation

The finite element code FIDAP is adopted for numerical simulations of the problem. FIDAP subroutines are modified to incorporate the full nongray radiation model, RAD I, and the approximate nongray model, RAD II. For the present reactor configuration, calculation of radiation viewfactors between the fiber and the quartz is unduly difficult, because the fiber length to diameter ratio is approximately 100. The FIDAP subroutine FACET is not able to produce sufficiently accurate viewfactors. Therefore, a separate subroutine was written to calculate all the necessary viewfactors from the cylinder to base relationship provided by Naraghi and Chung (1982). The resulting viewfactors conserve radiation energy to within 0.01%.

Isoparametric nine-node elements are used in both the solid and the fluid regions. Due to the logarithmic variation of the temperature in the transverse direction and because of the inlet and outlet effects, it is extremely important to have sufficient nodes near the fiber and in the entrance and exit regions of the reactor. Based on grid sensitivity analyses, a nonuniform 305 by 37 mesh is chosen. Further subdivision of the domain did not produce more accurate results. All the solutions presented here are steady-state results generated using a combination of successive substitution and Newton-Raphson solution techniques. Solution convergence is checked and satisfied, when both the norms of the residual vector and the normalized root mean square error for each dependent variable are below 0.1%. Unless specified otherwise, the full radiation model, RAD I, and the explicit dependence of density on temperature are used in the simulations presented in the next section.

Results and Discussion

In the first case examined here, the working fluid is hydrogen. It enters the reactor at a uniform flow rate of 1 slm and a uniform temperature of 300 K. The exit section of the reactor is also kept at a uniform temperature of 300 K (this condition is used for all the cases). The temperature of the fiber is assumed to be constant in time, but varies spatially as measured during the experiment, as shown in Table 1. The predicted wall temperatures for the fiber at around 1,722 K are presented in Figure 3 and compared to experimental measurements. To isolate the role of radiation heat transfer, three different theoretical curves representing different assumptions with regard to radiation heat transfer are presented. The solid line represents the prediction using the full nongray radiation model, in which radiation heat transfer between the fiber and the quartz wall, the quartz wall to itself, and the radiation loss to the surrounding are rigorously incorporated. The dashed line represents the case, in which radiation heat transfer between the quartz wall and the fiber is neglected, but radiation loss from the quartz wall to the surrounding is included. The dashed-dotted line represents the case, in which radiation heat transfer is totally neglected. The error bars indicate the uncertainty associated with the reproducibility of the measurements. The comparison indicates that the full-radiation and the no-fiber-radiation cases essentially predict the same wall temperature distributions which are also in good agreement with the experimental measurements. However, the no-radiation case overpredicts the measured values significantly. Similar results were obtained for a fiber temperature around 1,421 K, as shown in Figure 4. This obviously indicates that for hydrogen, because of its relatively high conductivity, conduction is the main mode of heat transfer to the wall, and radiation serves mainly as a cooling mechanism as the heated quartz wall emits to the surrounding environment. This finding is not intuitively

Table 1. Experimentally Measured Fiber Temperature

Fiber Temp. K	1 slm Hydrogen		1 slm Argon		0.05 slm Argon
Axial Location cm	$\bar{T}_{\text{fiber}} = 1{,}722$ K	$\bar{T}_{\text{fiber}} = 1{,}421$ K	$\bar{T}_{\text{fiber}} = 1{,}719$ K	$\bar{T}_{\text{fiber}} = 1{,}417$ K	$\bar{T}_{\text{fiber}} = 1{,}719$ K
1	1,694	1,369	1,662	1,371	1,653
2	1,707	1,391	1,679	1,387	1,679
3	1,715	1,402	1,690	1,393	1,7067
4	1,721	1,406	1,695	1,396	1,697
5	1,723	1,415	1,704	1,404	1,717
10	1,725	1,420	1,716	1,411	1,712
15	1,722	1,422	1,723	1,422	1,712
20	1,720	1,425	1,721	1,424	1,719
25	1,722	1,426	1,714	1,417	1,719

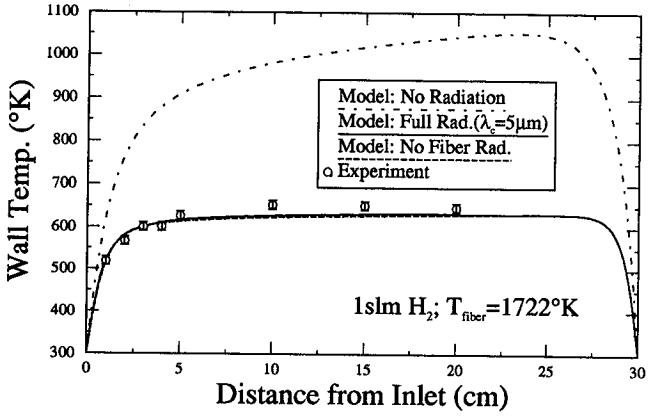

Figure 3. Comparison of predicted and measured wall temperature profiles for 1 slm hydrogen and fiber temperature of 1,722 K.

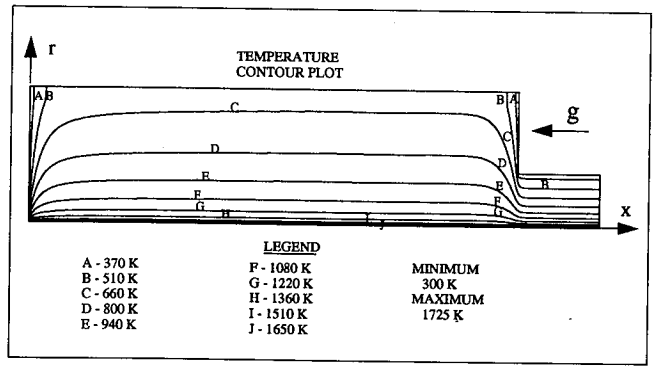

Figure 5. Predicted temperature contours for 1 slm hydrogen and fiber temperature of 1,722 K.

obvious, because, in these cases, the fiber is glowing hot (at a temperature of 1,722 K), while the wall is much cooler (at around 600 K).

The flow and temperature distributions in the reactor are presented in Figures 5-7 for T_{fiber} = 1,722 K. It is evident from the radial velocity profiles presented in Figure 6 that for hydrogen at 1 slm, there is only minor distortion of the flow near the inlet due to expansion and entrapment of the fluid in the top section of the reactor, but there are no signs of recirculation. Furthermore, the temperature contours in Figure 5 and the radial temperature profiles in Figure 7 indicate that because of the relatively high conductivity of the gas, fully developed temperature profiles are approached very rapidly (to within 3 to 5 cm from the inlet).

The next case examined is for argon which again enters the reactor at a uniform flow rate of 1 slm and a uniform temperature of 300 K. The two fiber temperature distributions for this case are included in Table 1. The wall temperature distributions predicted by the model for fiber temperatures around 1,719 K and the corresponding experimental results are presented in Figure 8. As was the case with hydrogen, there is excellent agreement between the full-radiation model and the experiment, while again the no-radiation case overpredicts the results. At this time, however, unlike the hydrogen case, the no-fiber-radiation case underpredicts the measured values. This suggests that because of the relatively low conductivity of argon, radiation heat transfer between the fiber and quartz contributes significantly to the heating of the quartz, and its omission results in underprediction of the wall temperature. It is obvious that there is a substantial difference between the magnitudes of the overprediction of the wall temperature by the no-radiation case and the underprediction of the wall temperature by the no-fiber-radiation case. This means that the wall loses more radiant energy to the surrounding than it receives from the fiber. Therefore, even for argon, radiation is still more important as a cooling mechanism for the reactor wall. The comparison of results for fiber temperature of 1,417 K in Figure 9 again corroborates these conclusions. Figures 8 and 9 also indicate that the no-fiber-radiation case underpredicts the wall temperatures near the entrance region, where the gas is relatively cold and therefore radiation from the fiber is the main source of heat transfer to the wall. However, the no-radiation case overpredicts the results nearer the middle of the enclosure, where the wall has reached a high-temperature plateau and therefore emission to the surrounding environment is important.

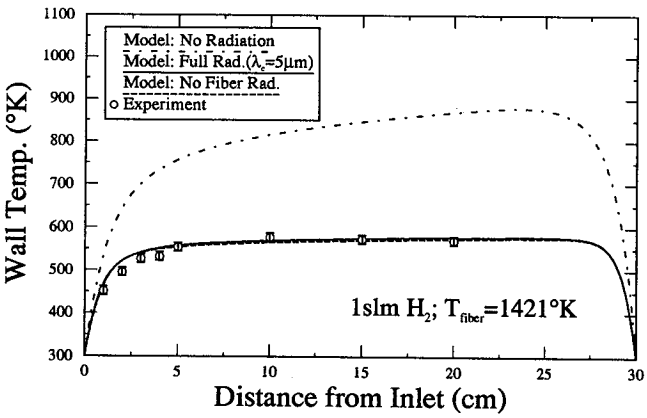

Figure 4. Comparison of predicted and measured wall temperature profiles for 1 slm hydrogen and fiber temperature of 1,421 K.

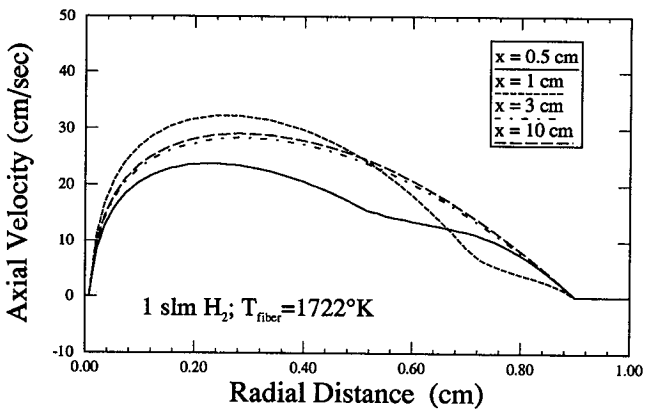

Figure 6. Predicted axial velocity profiles at several axial locations for 1 slm hydrogen and fiber temperature of 1,722 K.

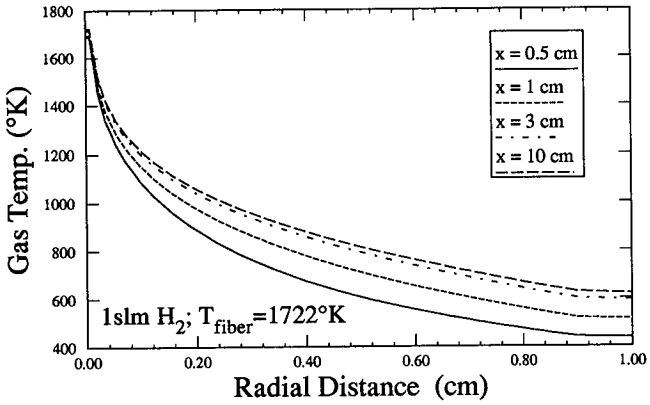

Figure 7. Predicted temperature profiles at several axial locations for 1 slm hydrogen and fiber temperature of 1,722 K.

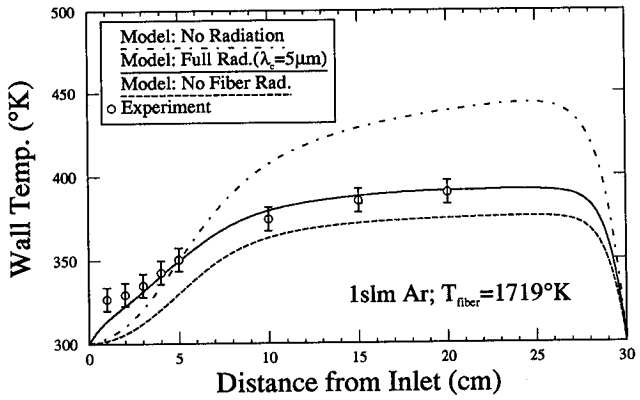

Figure 8. Comparison of predicted and measured wall temperature profiles for 1 slm argon and fiber temperature of 1,719 K.

The velocity and temperature fields for the argon case are presented in Figures 10–12. They indicate a recirculating natural convective flow which was absent in the hydrogen case. The radial velocity profiles of Figure 11 indicate that the natural convection effect intensifies the flow near the fiber and

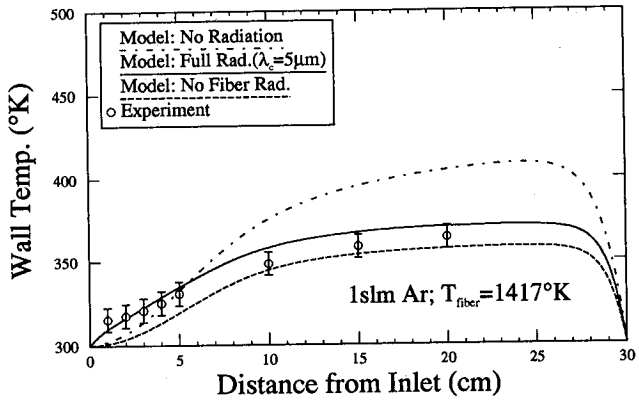

Figure 9. Comparison of predicted and measured wall temperature profiles for 1 slm argon and fiber temperature of 1,417 K.

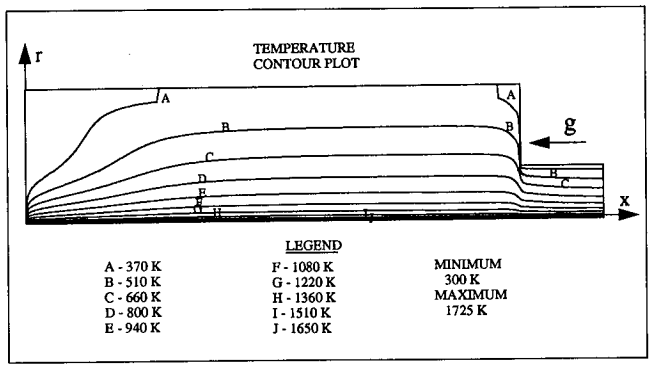

Figure 10. Predicted temperature contours for 1 slm argon and fiber temperature of 1,719 K.

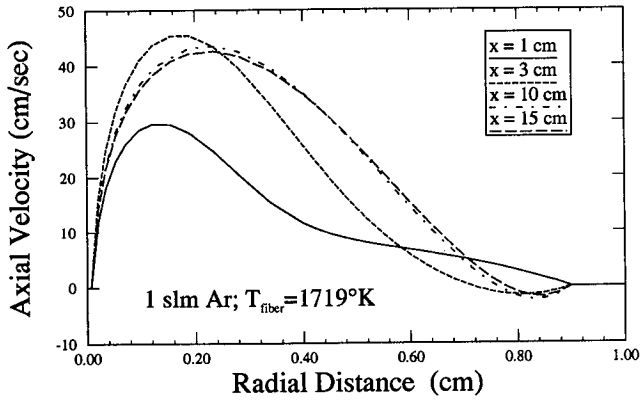

Figure 11. Predicted axial velocity profiles at several axial locations for 1 slm argon and fiber temperature of 1,719 K.

increases the residence time of the gas near the quartz wall, where a large, but weak, recirculating vortex ensues. Because of the low thermal conductivity of argon and the modification of the temperature field by the recirculating flow, the approach to a fully developed temperature profile is slower. The temperature contours in Figure 10 and the radial temperature profiles in Figure 12 indicate that fully developed temperature

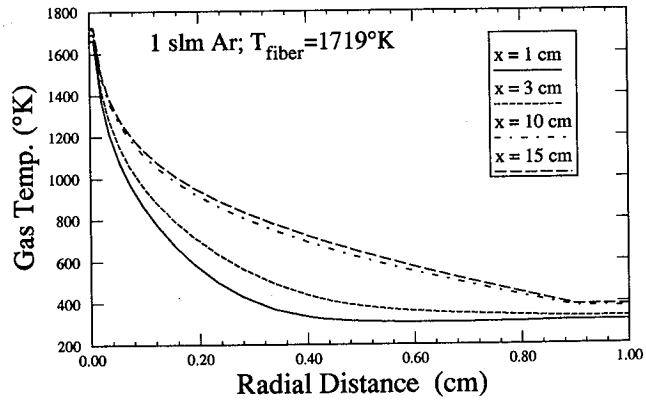

Figure 12. Predicted temperature profiles at several axial locations for 1 slm argon and fiber temperature of 1,719 K.

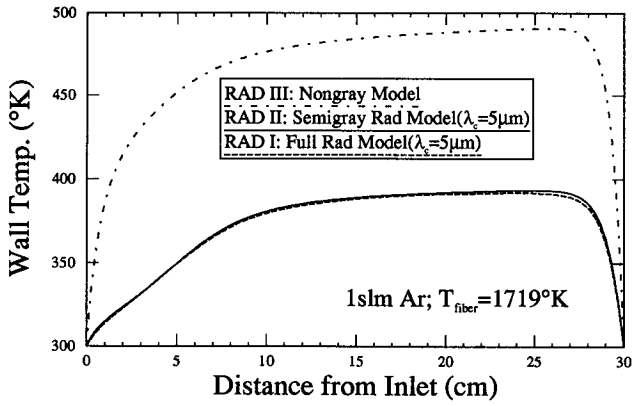

Figure 13. Comparison of wall temperature predictions by three different radiation models for 1 slm argon and fiber temperature of 1,719 K.

profiles are attained to within 10 cm from the inlet. The radial temperature distributions of Figure 12 also indicate the existence of weak *cold fingers* in the gas near the inlet ($x = 1$ cm and 3 cm). It refers to a situation where due to radiative transfer the quartz wall is at a higher temperature than the adjacent flowing gas. This effect is naturally more pronounced near the inlet, where the flow is not yet thermally developed and radiation is the dominant mode of heat transfer to the wall. Note that in the hydrogen case, which has a higher thermal conductivity, there is no evidence of *cold fingers* (compare Figures 7 and 12).

Multipurpose codes such as FIDAP are used to study CVD processes more frequently now than in the past. Unfortunately, the full nongray radiation model used in this article requires view factors and semigray analysis which are not readily available in these codes. Therefore, it is useful to see if radiation heat transfer in the quartz reactor can be predicted reliably using simpler radiation models which are not so computationally cumbersome. The test cases for these simpler radiation models, namely RAD II and RAD III, use argon at 1 slm, where radiation effects are more important. Comparison of wall temperature predictions of RAD III, RAD II, and the full model RAD I for fiber temperatures of 1,719 K and 1,417 K are presented in Figures 13 and 14, respectively. It is apparent that while the nongray model RAD III overpredicts the correct results significantly, the semigray model RAD II provides an excellent approximation to the full model. Indeed, the surprisingly close agreement between the predictions of RAD I and RAD II suggests that for the problem at hand, a detailed view factor calculation is not warranted. This stems from the following three facts:

1. The aspect ratio of the reactor is sufficiently large such that the view factors from fiber to quartz wall and from quartz wall to itself basically approach unity.
2. The temperature of the fiber is relatively uniform over a major portion of its length.
3. Wall temperatures are rather low compared to fiber temperatures.

Needless to say, these facts hold only for the reactor configuration and the fiber temperature distributions studied here. If the diameter to length ratio of the enclosure is increased or if the fiber temperature distribution becomes significantly nonuniform, the applicability and accuracy of the RAD II radiation model will accordingly decrease.

The significant discrepancy between the results predicted by the nongray model RAD III and the semigray models RAD II and RAD I suggest that the wavelength-dependent transmittance of quartz plays an important role in determining the wall temperatures. An important parameter, which controls the nongray behavior of quartz, is the cutoff wavelength. As depicted in Figure 2, the cutoff wavelength for quartz can vary from 3 to 5 micron. The sensitivity of the wall temperature to variations in the cutoff wavelength is shown in Figures 15 and 16 for fiber temperatures of 1,719 K and 1,417 K. In the 1,719 K case, the difference between the wall temperature predictions for cutoff wavelengths of 3 and 5 micron can be as large as 50°. Naturally, this sensitivity is decreased as the fiber temperature is lowered to 1,417 K. These results show that the cutoff wavelength is indeed an important heat-transfer parameter. This important consideration is often ignored in many areas of material processing such as CVD and crystal growth, where radiatively selective materials such as quartz or fused silica are routinely used in the experiments, but treated as either fully opaque or fully transparent in the analyses.

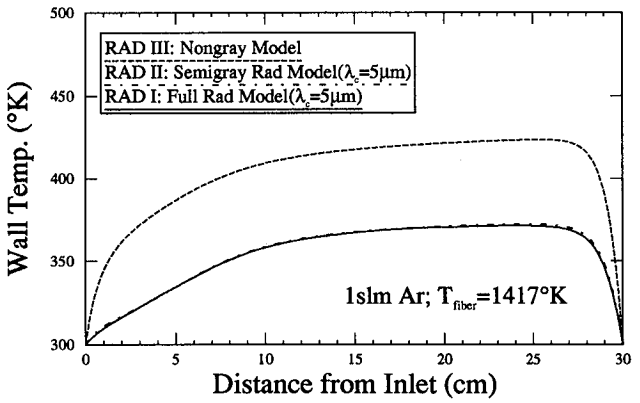

Figure 14. Comparison of wall temperature predictions by three different radiation models for 1 slm argon and fiber temperature of 1,417 K.

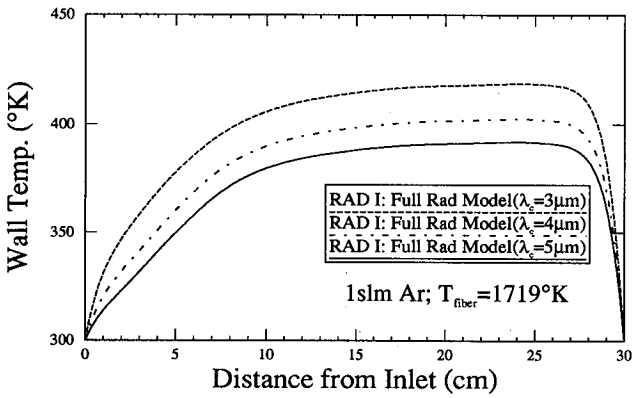

Figure 15. Effect of the cutoff wavelength on wall temperature predictions for 1 slm argon and fiber temperature of 1,719 K.

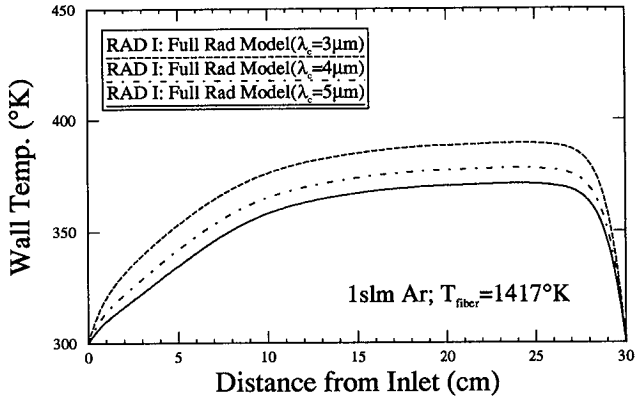

Figure 16. Effect of the cutoff wavelength on wall temperature predictions for 1 slm argon and fiber temperature of 1,417 K.

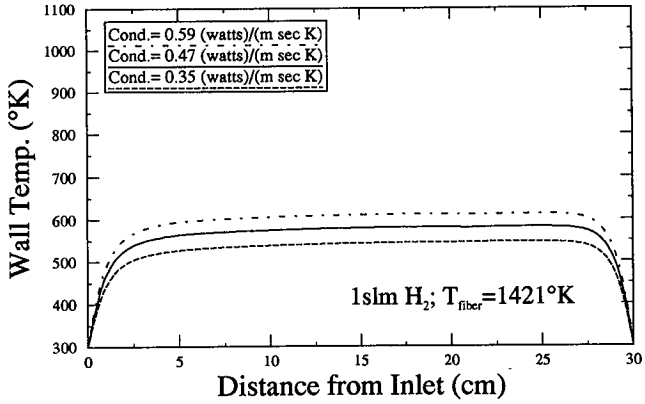

Figure 18. Effect of variations in thermal conductivity on wall temperature predictions for 1 slm hydrogen and fiber temperature of 1,421 K.

Our results show that in the CVD reactor, radiation and conduction are the dominant heat-transfer mechanisms. Therefore, it is also interesting to show the sensitivity of the wall temperature predictions to changes in thermal conductivity. Wall temperature predictions for argon are shown in Figure 17 for three different, but constant, thermal conductivities; an average value evaluated at the mean fully developed gas temperature, and high and low values obtained by changing the average conductivity by 25% (in all of the other results temperature-dependent thermal conductivities were used). Naturally, the average value gives the best overall agreement with the variable conductivity predictions and the experimental results (see Figure 8), except near the inlet where the temperature of the gas is significantly lower than the average fully developed temperature. Comparison between the Figures 15 and 17 also indicates that for argon, the wall temperature predictions basically exhibit the same sensitivity to a 25% change in cutoff wavelength as to 25% variation in thermal conductivity. This again confirms that for argon, radiation and conduction heat transfer are equally important and underlines the significance of the cutoff wavelength. Figure 18 shows the sensitivity of wall temperatures to 25% variation in thermal conductivity for the hydrogen case. These results again confirm that for

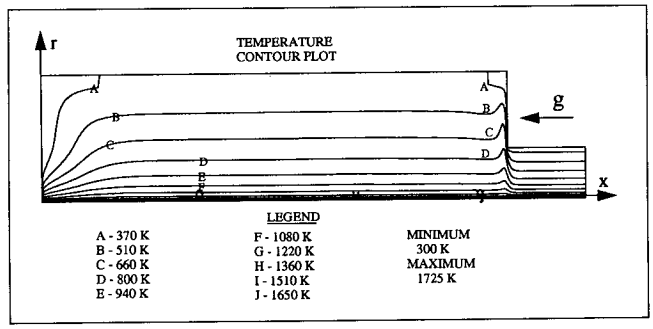

Figure 19. Predicted temperature contours for 0.05 slm argon and fiber temperature of 1,719 K.

hydrogen, because of its high thermal conductivity, wall temperatures are much more sensitive to variations in thermal conductivity than to any other assumptions with regard to radiative exchange between the fiber and the quartz wall.

Finally, to assess the validity of the Boussinesq approximation, argon at a slow flow rate of 0.05 slm is considered. This case is chosen because it is equivalent in mass flow rate to 1 slm hydrogen. The results in Figures 19–21 are obtained

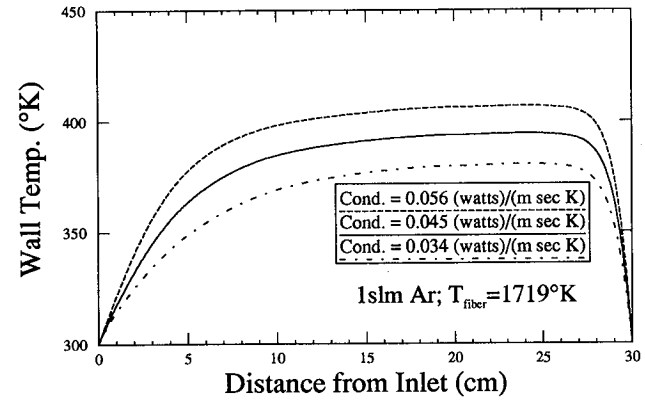

Figure 17. Effect of variations in thermal conductivity on wall temperature predictions for 1 slm argon and fiber temperature of 1,719 K.

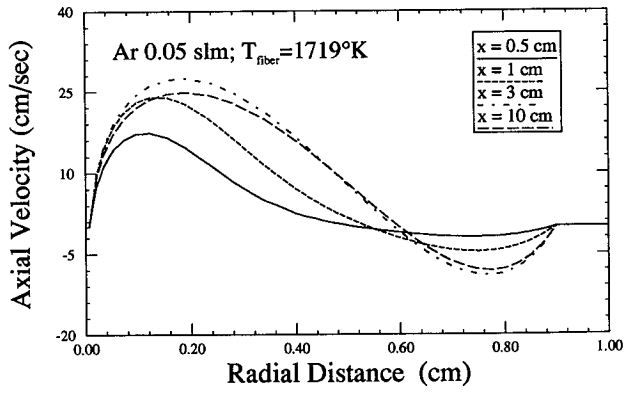

Figure 20. Predicted axial velocity profiles at several axial locations for 0.05 slm argon and fiber temperature of 1,719 K.

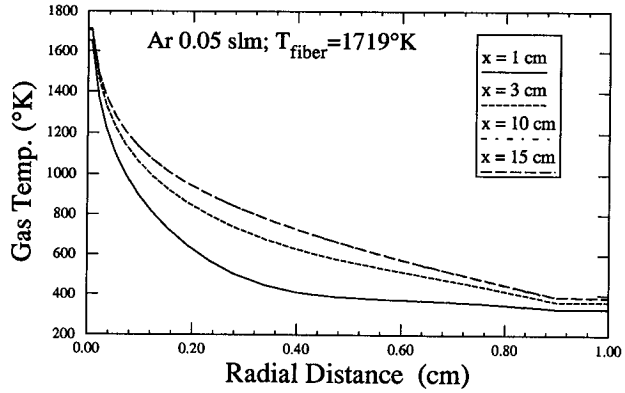

Figure 21. Predicted temperature profiles at several axial locations for 0.05 slm argon and fiber temperature of 1,719 K.

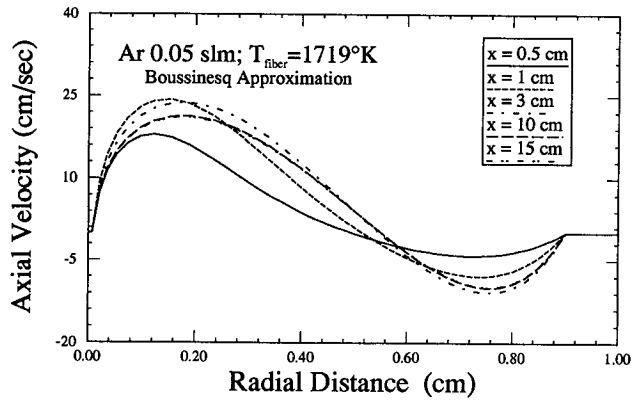

Figure 23. Predicted axial velocity profiles at several locations for 0.05 slm argon and fiber temperature of 1,719 K using Boussinesq approximation.

using the explicit variable-density model, while those in Figures 22–24 were obtained using the traditional Boussinesq approximation. The velocity profiles in Figures 20 and 23 indicate that the Boussinesq approximation, which takes into account only the density variations in the buoyancy term, predicts a weaker flow especially near the fiber. It also indicates that the flows predicted by the two models are slightly different especially at the inlet. The difference in velocities, however, is not sufficiently large to affect the gas and wall temperature distributions appreciably. As a result, the temperature contours presented in Figures 19 and 22 and the radial temperature profiles presented in Figures 21 and 24 are almost identical and unaffected by the different representations of density. In any case, because of the lower flow rate, these temperature profiles indicate a more rapid establishment of the fully-developed temperature field and an absence of the cold fingers in the gas.

Conclusions

As part of a continuing effort to develop a high-fidelity model for CVD processes, flow and heat transfer in a fiber growth reactor are studied numerically with special attention devoted to the effects of nongray-radiation heat transfer and natural convection. Comparison of numerical predictions with experimental measurements provides insight into the effects of the various interacting phenomena and reveals several interesting facts:

- When hydrogen is the working fluid, conduction is the dominant mode of heat transfer between the fiber and quartz wall, even at elevated fiber temperatures. In this case, radiation basically serves as a cooling mechanism for the reactor, as the heated wall emits to the surrounding environment.
- When argon is the working fluid because of its lower conductivity, radiation and conduction heat transfer from the fiber to the quartz wall are equally important. Hence, a correct treatment of radiation is essential for accurate temperature predictions.
- Because quartz is a radiatively selective material, a spectral treatment of radiation heat transfer in the CVD reactor is required. The cutoff wavelength is an extremely important heat-transfer parameter which must be correctly specified if accurate wall temperature predictions are desired.
- In cases where the aspect ratio of the reactor is sufficiently large and the fiber temperature is relatively uniform (such as the case studied here), radiation heat transfer between the fiber

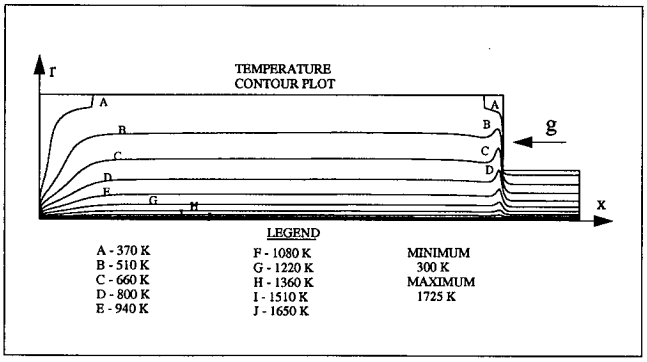

Figure 22. Predicted temperature contours for 0.05 slm argon and fiber temperature of 1,719 K using the Boussinesq approximation.

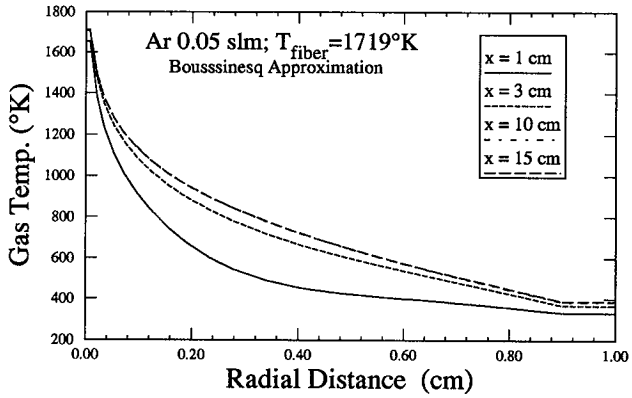

Figure 24. Predicted temperature profiles at several axial locations for 0.05 slm argon and fiber temperature of 1,719 K using Boussinesq approximation.

and quartz wall can be adequately modeled as exchange between two infinite concentric cylinders.

• The recirculating flow caused by natural convection is stronger when argon is the working fluid, especially at lower flow rates. For these cases, the flow predictions obtained using the variable-density model differ slightly from the ones obtained using the Boussinesq approximation. However, the temperature predictions are not sensitive to these density variations.

Acknowledgment

The valuable assistance of Mr. Ron Gaug in system-related and post processing issues and the support of the Computational Materials Laboratory in the Processing Science and Technology Branch are gratefully acknowledged.

Notation

A = surface area, m^2
c_p = heat capacity, $W/kg \cdot K$
D = diameter of the enclosure, m
g = gravitational acceleration, m/s^2
H = incident radiation flux, W/m^2
h_c = coefficient of convective heat transfer, $W/m^2 \cdot K$
k = thermal conductivity, $W/m \cdot K$
K = radiation viewfactor kernel, $1/m^2$
L = length of the enclosure, m
n = unit normal vector
p = pressure, N/m^2
Pr = Prandtl number
r = radial coordinate, m
r, r' = position vectors
Ra = Raleigh number
T = temperature, K
u = velocity vector, m/s
W = surface radiosity, W/m^2
x = axial coordinate, m

Greek letters

β_T = coefficient of thermal expansion, 1/K
ϵ = surface emissivity
μ = dynamic viscosity, $kg/m \cdot s$
ρ = density, kg/m^3
σ = Boltzmann constant, $W/m^2 \cdot K^4$

Subscripts

o = reference values
f = pertaining to the fiber
w = pertaining to the walls
∞ = pertaining to the surrounding

Literature Cited

Alam, M. K., and V. Puneet, *Simulation of Fiber Coating CVD Reactor*, ASME HTD-184, p. 99 (1991).

Gokoglu, S. A., "Chemical Vapor Deposition Modeling—An Assessment of Current Status," *Chemical Vapor Deposition XI*, K. E. Spear and G. W. Cullen, eds., Electrochem. Soc., p. 1, Also NASA CR-185301 (1990).

Gokoglu, S. A., M. Kuczmarski, L. Veitch, P. Tsui, and A. Chait, "A Numerical and Experimental Analysis of Reactor Performance and Deposition Rates for CVD on Monofilaments," *Chemical Vapor Deposition XI*, K. E. Spear and G. W. Cullen, eds., Electrochem. Soc., p. 31 (1990).

Gokoglu, S. A., W. A. Arnold, P. Tsui, and A. Chait, "Prediction of 2-D Convection Effects and Deposition Rates in a Reactor Configured for CVD on Single Fibers," *Transport Phenomena in Manufacturing*, ASME FED-90, p. 9 (1989).

Gokoglu, S. A., "Chemical Vapor Deposition Modeling for High Temperature Materials," *Proc. of Materials Research Society Fall Meeting, Symposium R: Chemical Vapor Deposition of Refractory Metals and Ceramics II*, Besmann et al., eds., Mat. Res. Soc. Symp. Proc., **250**, p. 17, Also NASA TM-105386 (1991).

Jensen, K. F., "Microelectronics Processing: Chemical Engineering Aspects," *Advances in Chemistry Series*, D. W. Hess and K. F. Jensen, eds., Amer. Chem. Soc., Washington, DC, No. 221, p. 199 (1989).

Holland, L. R., "A Thermal Transmission Function for Fused Silica Ampoules," *J. of Crystal Growth*, **49**, 426 (1980).

Lienhard, J. H., *A Heat Transfer Textbook*, Prentice-Hall, Englewood Cliffs, NJ (1981).

Naraghi, M. H. N., and B. T. F. Chung, "Radiation Configuration Factors Between Disks and a Class of Axisymmetric Bodies," *J. of Heat Transfer*, **104**, 426 (1982).

Scholtz, J. H., and V. Hlavacek, "CVD Reactors for the Coating of Fibrous Substrates: Modeling and Numerical Simulation," *J. Electrochem. Soc.*, **137**(11), 3459 (1990).

Scholtz, J. H., J. E. Gatica, H. J. Viljoen, and V. Hlavacek, "Coating of Fibrous Substrates by CVD; Analysis of the Fiber Evolution," *J. Crystal Growth*, **108**, 190 (1991).

Manuscript received Aug. 31, 1992, and revision received Mar. 23, 1993.